IJE TRANSACTIONS A: Basics Vol. 37 No. 07, (July 2024) 1263-1273

International Journal of Engineering

Journal Homepage: www.ije.ir

An Innovative and Reliable Hybrid Cooling Method for Electric Vehicle Motors

J. Selvan[a], S. Manavalla*[b]

[a] *School of Mechanical Engineering, Vellore Institute of Technology Chennai, India*
[b] *Electric Vehicles Incubation, Testing and Research Centre, Vellore Institute of Technology Chennai, India*

PAPER INFO

Paper history:
Received 05 November 2023
Received in revised form 14 December 2023
Accepted 30 December 2023

Keywords:
Electric Vehicle Motor Cooling
Phase Change Material
Computational Fluid Dynamics

ABSTRACT

Air, liquid, and oil are commonly used for the cooling of electric vehicle motors. Phase change materials (PCM) are not extensively used apart from electronic components. In general, coolants like air, liquid, and oil were separately used as independent coolants for the motor. In this research, two cooling channels were added to the motor cooling. The liquid is used as a primary coolant, while PCM is used as a secondary coolant. This novel method of cooling helps to keep the bracket temperature under the allowable limit even though the liquid cooling is operating at its lowest operating point. In the study, the primary focus was on the PCM coolant channel by keeping the liquid coolant under one particular operating condition to study the PCM in detail. The thickness of the PCM had an influence on the motor cooling. Three different PCM channels were studied with thicknesses of 6 mm, 8 mm, and 10 mm. The best cases were identified with a 6 mm PCM thickness, which is better in terms of heat transfer improvement of 6% observed.

***doi**: 10.5829/ije.2024.37.07a.06*

Graphical Abstract

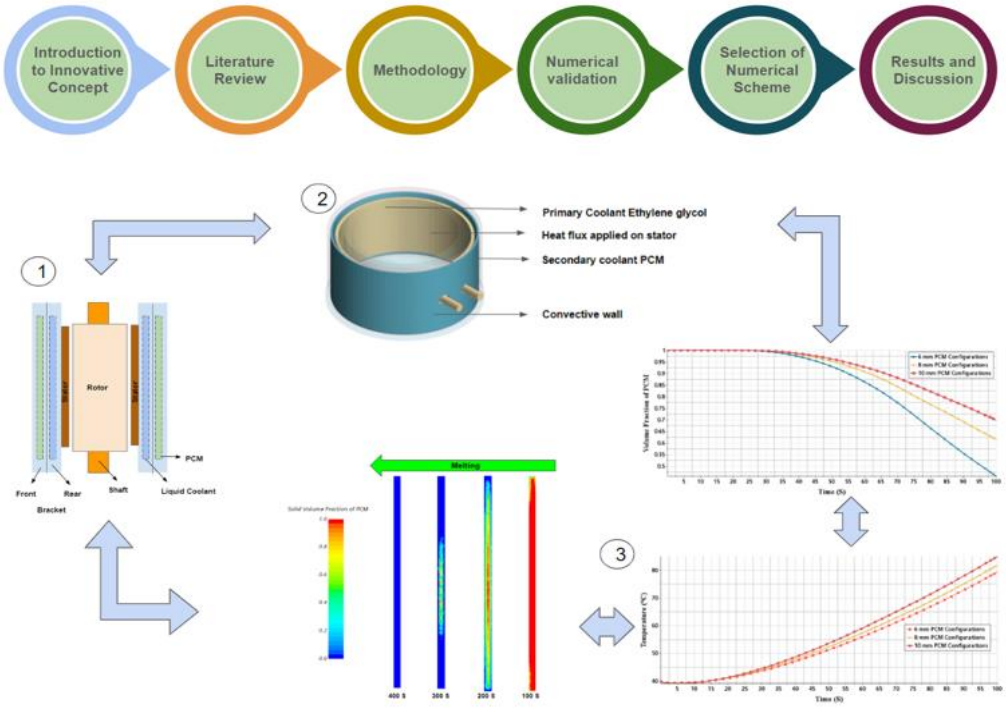

*Corresponding Author Email: manavalla.sreekanth@vit.ac.in (S. Manavalla)

Please cite this article as: Selvan J, Manavalla S. An Innovative and Reliable Hybrid Cooling Method for Electric Vehicle Motors. International Journal of Engineering, Transactions A: Basics. 2024;37(07):1263-73.

NOMENCLATURE

A_{mush}	mushy zone (m^2)	$\vec{v}$	fluid velocity (m/s)
c_p	Specific heat at constant pressure J/(kg °C)	β	liquid volume fraction
h_{ref}	Reference enthalpy (J)	ε	constant
h	Sensible enthalpy (kJ)	ρ	Density (kg/m³)
ΔH	latent enthalpy (J)	$\overrightarrow{v_p}$	solid velocity (m/s)
L	Liquid	φ	turbulence parameter
S	Source term		

1. INTRODUCTION

In recent years, electric vehicles (EVs) have gained significant popularity and have become a hot topic in the automotive industry. This surge in interest can be attributed to several factors, including the growing concern for the environment, the need to reduce dependence on fossil fuels, and advancements in technology. EVs offer a promising solution to these challenges by providing a cleaner and more sustainable mode of transportation.

Motor thermal management plays a crucial role in ensuring the optimal performance and longevity of electric vehicle motors. As electric motors convert electrical energy into mechanical energy, they generate heat as a byproduct. Excessive heat can have detrimental effects on the motor's efficiency, reliability, and overall performance. Therefore, effective thermal management is essential to maintaining the motor within the appropriate temperature range.

The basic functional requirements of any automobile vehicle that would be expected from the customer's side are

- Acceleration
- High energy and fuel economy while traveling
- Maximum speed, speed control and ride comfort
- Minimum filling/recharge time of fuel or energy
- Minimum pollution while running
- Longer Vehicle/Battery Life

The drive cycle of a fuel-powered automobile or electric vehicle (EV) completely depends on traffic conditions, road conditions, road terrain, and the load carried by the vehicle. The drive cycle also depends on the various inputs from the driver based on the road conditions. The running of an EV also affects the working condition of the electric motor, which needs to undergo frequent sudden stoppages, high acceleration, and deceleration, along with different environmental conditions. Electric motors in industrial applications operate at rated speeds and under rated conditions. Thus, the industrial electrical motor design approach cannot be applied to electric vehicles. Electric motors used in e-vehicles must meet the basic vehicle requirements for efficient operation (1).

Computational fluid dynamics (CFD) can provide detailed studies of fluid flow that cannot be obtained analytically or experimentally. Since CFD models, which have demonstrated compelling performance, can save money on prototype manufacturing. CFD has become very popular since the introduction of high-speed computing, it is necessary to use either experimental or CFD simulation for flow visualization. Flow visualization using transparent materials was attempted earlier. Although it is simple and inexpensive, it is not suitable for colorless gases such as air. In such cases, CFD simulations can be used to visualize the flow.

Using analysis, Bellettre et al. studied (2) a model in transient state for an auto-synchronous e-machine stator and identified problematic locations on the copper winding, leading to the selection of a phase change material as the cooling system. The conventional method of testing induction motors, as analyzed by Huai et al. (3); therefore, it is becoming more important to use mathematical modeling tools and computational experiments to estimate temperature rise. This is especially relevant in the thermal study of electrical machines. Boglietti et al. (4)performed extensive surveys on the history and current approaches. The developments and the latest methods introduced over the last decade are examined in detail and contrasted to demonstrate their strengths and shortcomings. Hosain and Fdhila (5) optimized design parameters for inlet and groove geometry to increase cooling performance. Yabiku et al. (6) proposed a technique for measuring the rise in temperature of critical sections of induction e-machines under stop and start conditions by accounting for the impact of material. Cavazzuti et al. (7) introduced a powerful brushless synchronous e-machine with magnets to conduct a thermal analysis using a lumped parameter approach. Research by Kuria and Hwang (8) explains three-dimensional CFD simulations conducted over a fan-cooled brushless DC motor in a fully enclosed environment. The machine was analyzed to determine the temperatures of the critical machine components and the effects of various thermal parameters. Kim et al. (9), Kim and Kim (10), and Kim (11) suggested a few design points to enhance the E-machine thermal design and then verified the improvement of the cooling efficiency. Nategh et al. (12) conducted simulations to analyze the flow of fluids in the cooling channels by using partial modeling. The output of the numerical simulation is used as feedback to the lumped parameter approach, which will explain the transfer of heat to the fluid. He found the approaches useful because of their simplicity, since complete machine analysis is avoided. Zhou et al. (13) used a technique to construct efficient and robust electrical machine thermal models that were used for real-time thermal observation and modeling.

According to Lim and Kim (14), the solid shaft of a 35 kW high-capacity wheel e-channel machine's design was examined for oil splash cooling and numerical analysis and practical testing were used to assess the machine's cooling efficiency. Huang et al. (15) provided heat transfer modeling of a high output brushless e-machine with rotor magnets and heat pipes with liquid cooling passage. Pechánek and Bouzak (16) used CFD to analyze the two water jackets for the e-machine cooling system and explained how heat transfer can be enhanced. Li (17) proposed a numerical model for solving the thermal problem, and the developed model is in good agreement with the experiments.

Jayakumar and Sreekanth (18) discussed the novel approach of cooling an e-machine using a baffle and its arrangements. Selvan and Manavalla (19) studied the phase-change material as the primary coolant for cooling the e-machine and discussed its practical feasibility. The PCM as a secondary coolant for the motor cooling was not studied in detail before, and either liquid coolant or oil coolant was used in the past for the cooling. In this study, we are going to introduce a new concept in the cooling of the motor by adding two different cooling channels to protect the motor from overheating. The primary coolant is the liquid coolant, and the secondary coolant is the PCM. The secondary coolant is introduced to protect the motor when the liquid coolant is running at lower flow rates or in the event of coolant pump failure. The secondary coolant is the primary focus of this study, and it is thoroughly investigated to understand its impact on the overall system.

Table 1 gives an overview of cooling methods applied by different researchers and engineering techniques to design the cooling system. Most of research focus on the air cooled machine followed by liquid, oil, heat pipe and design optimization, testing were carried out using analytical, experimental & CFD/FEA.

Phase change materials (PCM) have not been thoroughly investigated as a cooling medium for e-machines. This study investigates the OM35 PCM [20] as a coolant for the stator and brackets to assess the benefits of PCM. Phase Change Materials (PCMs) are substances that can store and release thermal energy during the process of melting and solidification. While PCMs offer several advantages such as high-energy storage density and long-term stability, they also have a few drawbacks that make them less desirable in certain applications. By highlighting these drawbacks, we can better understand why OM35 is a preferred choice.

OM35, a specific PCM, addresses some of these drawbacks. It has a wide operating temperature range (-35°C to 35°C), high thermal conductivity, and minimal super cooling and sub cooling effects. Additionally, OM35 exhibits minimal volume change during phase transition and demonstrates good cycling stability. These features make OM35 a favorable choice for various applications, including economical operation, building insulation, energy storage systems, and thermal

TABLE 1. Cooling method and engineering analysis technique used by various researchers

Reference	Cooling method				Engineering analysis technique			
	Air	Liquid	Oil	Heat Pipe	Lumped/ Mathematical	Experimental	CFD/FEA	Motor rating, kW
Lee et al. (1)	×	×	✓	×	×	✓	✓	16.7
Bellettre et al. (2)	×	✓	×	×	×	✓	✓	-
Huai et al. (3)	✓	×	×	×	✓	×	×	1.5
Boglietti et al. (4)	✓	×	×	×	✓	×	✓	-
Hosain and Fdhila (5)	✓	×	×	×	×	×	✓	-
Yabiku et al. (6)	✓	×	×	×	✓	×	×	16
Cavazzuti et al. (7)	✓	×	×	×	✓	×	×	-
Kuria and Hwang (8)	✓	×	×	×	×	✓	✓	-
Kim et al. (9)	✓	×	×	×	×	✓	✓	10,25
Kim and Kim (10)	✓	×	×	×	×	✓	✓	-
Kim (11)	✓	×	×	×	×	✓	✓	5
Nategh et al. (12)	✓	✓	×	×	✓	✓	✓	4
Zhou et al. (13)	✓	×	×	×	×	✓	✓	145
Lim et al. (14)	×	×	✓	×	×	✓	✓	35
Huang et al. (15)	✓	✓	×	✓	✓	×	✓	-
Pechanek and Bouzak (16)	×	✓	×	×	×	✓	✓	-
Li et al. (17)	✓	×	×	×	×	✓	✓	-
Jayakumar and Sreekanth (18), Selvan and Manavalla (19)	×	✓	×	×	×	✓	✓	18

management. Other applications that use hybrid cooling applications such as "air-cooled condensers, cooling towers, surface condensers, and air-cooled heat exchangers", which were considered hybrid cooling.

The aim of this paper is to determine if the PCM can be utilized for cooling the e-machine. From the literature review so far, studies on e-machines have primarily been based on a liquid cooling system. To the best of our knowledge, PCM, along with a liquid coolant, was never studied earlier. Thus, in this article, PCM, is along with a coolant, is included in the bracket to enhance heat transfer, and its performance is studied.

2. GEOMETRY

The geometry consisting of the front and rear brackets, coolant passage, and stator stack. Figure 1 shows the schematic sketch of the proposed cooling method. To simplify the CFD analysis, only the components needed for bracket cooling are considered. The front and rear brackets hold the primary and secondary coolants, respectively.

The secondary coolant is where the innovation begins by adding the extra coolant to prevent the motor from overheating when the primary coolant is unable to adequately cool the motor or the pump is unable to deliver the coolant.

A heat source of 18 kW (19) was applied to the stator stack at an ambient temperature of 40 °C. The brackets were applied with a convective heat transfer coefficient of 10 W/m2K, as shown in Figure 2. The primary coolant of 0.01 kg/s was supplied, and the secondary coolant of PCM thickness was varied from 6 mm to 10 mm, as shown in Figure 3.

The bracket consists of primary and secondary coolants as shown in Figure 1. The primary coolant jacket is filled with the liquid coolant, and the secondary coolant is filled with PCM. The rotating system consists of a rotor and a shaft. The stator stack is assembled inside the brackets.

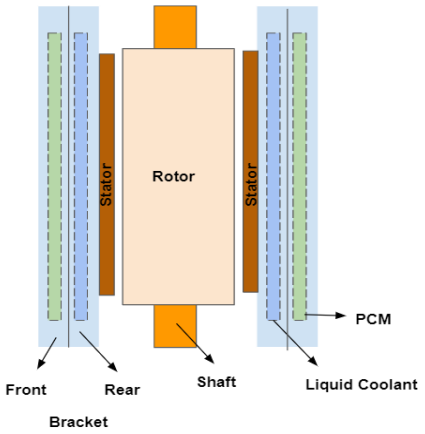

Figure 1. Schematic sketch of the cooling concept

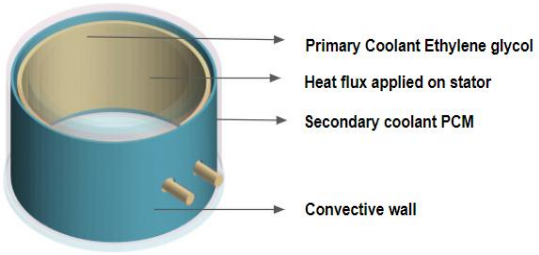

Figure 2. Simplified model of E-machine

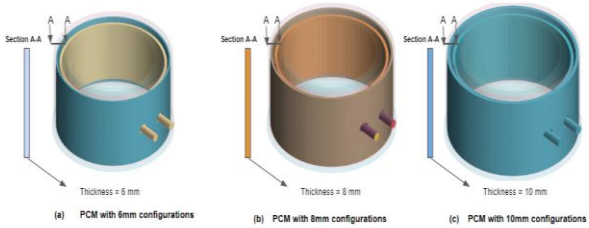

Figure 3. PCM Coolant configurations

3. CONCEPT OF TWO DIFFERENT COOLING CHANNELS

The intention behind this proposed cooling system is to improve the heat transfer of the front bracket. The advantage of improving the heat transfer of the front bracket is that it will help to improve inverter cooling where the inverter is mounted on the top of the front bracket. In general, the temperatures in the brackets are roughly between 180 - 200 °C while using primary coolant alone in the system (18, 19). With the proposed method, we can reduce the operating temperatures of the brackets, which will help the inverter's operating temperature be lower. In order to simplify the analysis, the inverter is not considered in this simulation, and it is assumed that lowering the bracket temperature will help the inverter electronics cooling.

The main goal of this research is to analyze how the PCM behaves in terms of absorbing and releasing heat when placed inside the bracket, as depicted in Figure 4. The speed at which the phase change occurs directly affects the heat transfer capability of the surroundings. To avoid manufacturing constraints and excessive costs, a minimum PCM thickness of 6 mm has been chosen. Going below this threshold would result in higher manufacturing costs. Therefore, this study focuses on numerical analysis and does not include thicknesses below 6 mm.

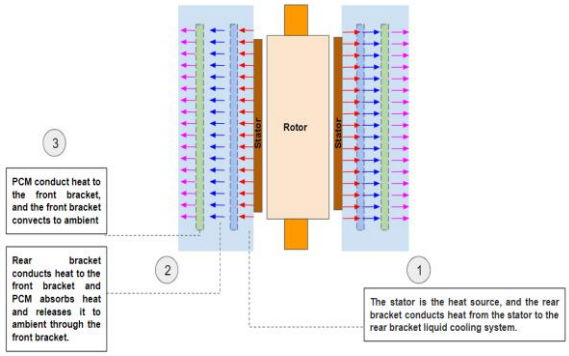

Figure 4. Concept of two different cooling system

4. METHODOLOGY

STAR-CCM+ models the solidification or melting process using an enthalpy method. The melt interface is not specifically tracked in this method. Instead, each cell in the domain has a value that separates the solid and liquid fractions present in the cell volume. At every iteration, the ratio of the medium is calculated using an enthalpy balance.

The "pseudo" porous medium that represents the mushy zone has a porosity that ranges from 1 to 0 when the substance solidifies. The porosity is zero when the material has entirely solidified in a cell, which causes the velocities to likewise be zero.

Enthalpy of a material is given by,

$$H = h + \Delta H \tag{1}$$

where,

$$h = h_{ref} + \int_{T_{ref}}^{T} c_p \, dT \tag{2}$$

The Latent Heat content can now be written in terms of the latent heat of the material, L:

$$\Delta H = \beta L \tag{3}$$

The latent heat content can vary between zero (for a solid) and L (for a liquid).

For solidification/melting problems, the energy equation is written as

$$\frac{\partial}{\partial t}(\rho H) + \nabla.(\rho \vec{v} H) = \nabla.(k \nabla T) + S \tag{4}$$

The momentum sink due to the reduced porosity in the mushy zone takes the following form: The momentum sink in the mushy zone is a result of the reduced porosity in that region. This reduced porosity affects the flow of momentum through the mushy zone, leading to a sink in momentum. The specific behavior and characteristics of the momentum sink in the mushy zone can vary depending on the specific situation and conditions. The momentum sink depends on the liquid volume fraction β of the mushy zone area with respect to its relative velocity (20).

$$S = \frac{(1-\beta)^2}{(\beta^2+\varepsilon)} A_{mush}(\vec{v} - \overrightarrow{v_p}) \tag{5}$$

$$S = \frac{(1-\beta)^2}{(\beta^2+\varepsilon)} A_{mush}\varphi \tag{6}$$

5. NUMERICAL VALIDATION OF CFD RESULTS WITH EXPERIMENT

The phase change of PCM was validated with experimental results to ensure the CFD results are logical and the results can be used for further research. The numerical model was tested by experiments, and a publication related to this research topic was found to validate the results. Pradeep and Venugopal (21) include experimental findings that closely resemble the scenario we are attempting to replicate. This scenario involves applying a heat source to a solid material and utilizing phase change material (PCM) to enhance the cooling process. The boundary condition is similar to the experimental setup (21) used to validate the numerical scheme. The temperature probes T1 to T8 were monitored and compared to validate the results, as shown below in Table 2 and Figure 5.

6. GRID AND TIME STEP INDEPENDENCY STUDIES

The solution obtained from the studies should be independent of the grid and time step. To confirm this, separate analyses were carried out for different grid sizes. For time dependency studies, different time steps were studied by monitoring the temperature as the field variable. The grid's independence was initially established for a grid size of 7 million cells. Beyond this, the grid was independent of bracket temperature for this study, as shown in Figure 6. After that, the time step was varied in steps of 0.001 s, and the bracket temperature was monitored. For a time step of 0.002 s and lower, the temperature remained the same as shown in Figure 7. Polyhedral cells were used, as shown in Figure 8.

TABLE 2. Comparison of temperatures as measured by Pradeep and Venugopal (21) and computed in the present work

Temperature Probe	Experiment	CFD	Deviation from Experiment, %
T1	55 °C	57 °C	3.64%
T2	48 °C	50 °C	4.17%
T3	27 °C	25 °C	7.41%
T4	27 °C	25 °C	7.41%
T5	27 °C	25 °C	7.41%
T6	27 °C	26 °C	3.70%
T7	27 °C	26 °C	3.70%
T8	27 °C	26 °C	3.70%

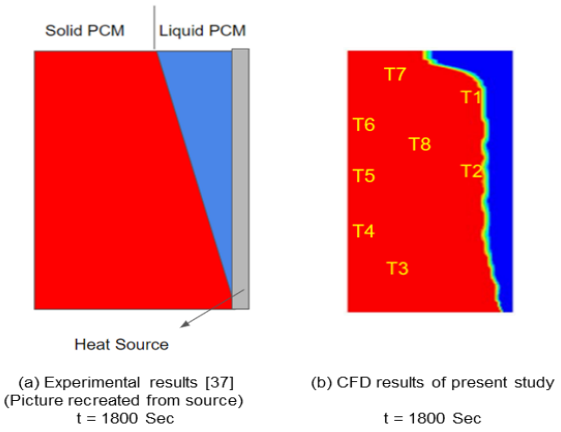

Figure 5. Comparison of CFD and Experimental results

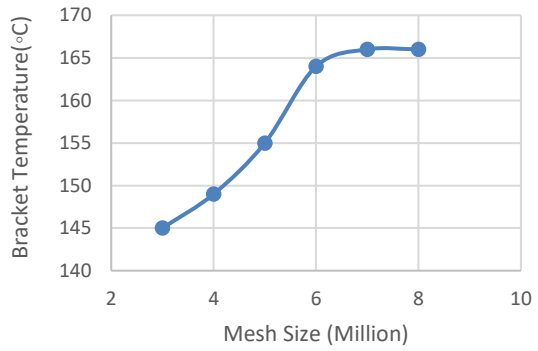

Figure 6. Results of grid independence study

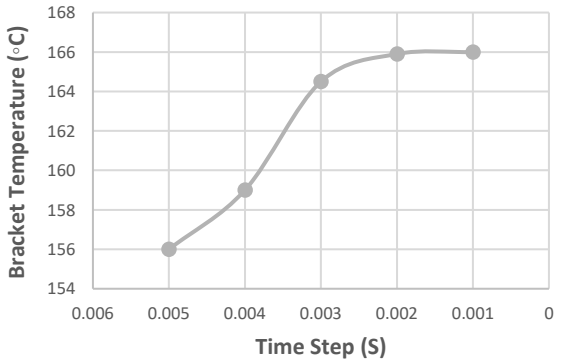

Figure 7. Results of time step independence study

7. NUMERICAL SCHEME SELECTION

In the present study, in order to simulate the change of phase, the multiphase unsteady solver was selected. Polyhedral mesh elements are used to capture the change of phases. Further, the multiphase solver with melting and solidification schemes was used to capture the melting process. The solidification process was not captured in this study. OM35 PCM was used as a secondary coolant, and for the primary coolant, ethylene glycol was used. The material properties are shown below in Table 3 (19, 21). The volume of fractions and the temperature of brackets were monitored for convergence. Along with this continuity, momentum and energy equation residuals are monitored for convergence of 1e-2.

8. RESULTS AND DISCUSSION

To understand the effect of primary and secondary coolant systems on the e-machine, the following parameters were monitored: The primary coolant is the liquid coolant system, where the inlet and outlet temperatures were monitored, and for the secondary cooling system, the PCM was monitored with respect to volume fraction and bracket temperature. Along with it, several PCM configurations' heat capacities were compared. Based on the above parameters, the best performing configurations were run under cyclic load conditions. In this analysis, we examined the fluctuating operating conditions and heat load of the machine, which is known as a cyclic load. To understand the complete thermal distribution along the PCM and liquid coolant passage, the unwrap section was used to show the temperature distribution between the inlet and outlet. The primary liquid coolant was kept at the lowest flow rate of 0.01 kg/s by assuming that the secondary coolant should protect the machine in the event the primary coolant fails because of pump failure.

8. 1. Different PCM Configurations are Compared for Volume Fraction The different PCM configurations were compared with respect to the volume fraction of PCM over a period of time, as shown in Figure 9. The y axis shows the volume fraction of PCM and the x axis shows the time period. The unsteady simulations were run for a period of 100 s. This is to understand the best performing PCM configurations. After that, real world conditions were simulated by applying the cyclic load conditions.

TABLE 3. Material properties of the coolant (21, 22)

Properties	OM35	Ethylene glycol (Ethane-1,2-diol)
Melting temperature (°C)	46.5	-
Density–Solid (kg/m^3)	747	-
Density–liquid (kg/m^3)	709.5	1060
Specific heat–Solid (J/kg.K)	1650	-
Specific heat–liquid (J/kg.K)	2219	4182
Thermal conductivity–S, (W/m.K)	0.17	
Thermal conductivity–L, (W/m.K)	0.16	0.26
Viscosity–(kg/m.s)	0.01602	0.01983

The PCM is used as a secondary coolant on the rear bracket. As discussed before, the primary coolant will take on the heat load, and the excess heat will be transferred into the PCM, which will act as a secondary coolant to protect the outer casing. So it is very clear that the PCM remains solid for 30 s, as shown in Figure 9. The primary coolant is taking the heat load up to 30 s. After that, the excess heat is transferred to the PCM and the phase change starts at 30 s. In this case, three different configurations were studied with different PCM thicknesses of 6 mm, 8 mm, and 10 mm. The phase change is fastest in 6 mm configurations, followed by 8 mm, and slowest in 10 mm configurations. The initial temperature of PCM is 40 °C, and once it reaches 44 °C, the phase change of PCM begins with a 2% volume change for 6 mm and less than a 1% change for the remaining configurations. After 50 s, only 8% of PCM converts into liquid, and the remaining 92% of PCM remains solid for 6 mm configurations, and for 8 mm and 10 mm configurations, this remains less than 5%. From 50s until 60s, there is a faster change of phase in the PCM with an additional 10% change. This continues for 100 s, and it is very linear progress for PCM in 6 mm configurations, whereas this is not observed in 8 mm or 10 mm. At 100 s, the 6 mm configurations transform into 50% PCM liquid, whereas the other configurations at 40% and 30% phase change do not. Based on the results, 6 mm of PCM performs better in a given time period when compared with other configurations.

The PCM remains almost solid for 30 s, and the section view in Figure 10 shows the phase change starting from the corner of the PCM and later progressing to the center. At 50 s, the phase change happens at the top and bottom corners faster compared to the center. Until 50 s, the change in volume of PCM is very minimal. After 50 s, the phase change is faster, and at the end of 100 s, over 50% of the PCM has been transformed into liquid. The 6 mm configurations of PCM are faster for the phase change, which is better for the heat transfer.

The volume fractions of 8 mm and 10 mm PCM thickness are shown in Figures 11 and 12 respectively. The phase change was not happening until 30 s, which is almost negligible. After 30 s, the phase change starts, which is slower in both the 8 mm and 10 mm configurations. The phase change pattern looks similar to 6 mm configurations, but it is slower by 5 to 10 % throughout the time period.

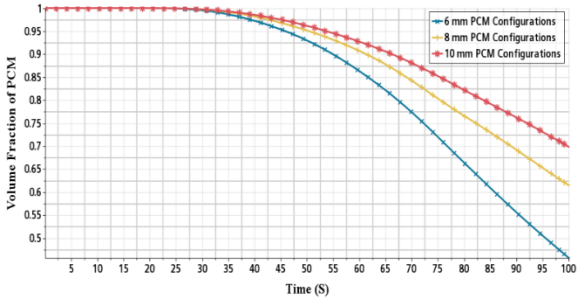

Figure 9. Different PCM configurations are compared for volume of fraction

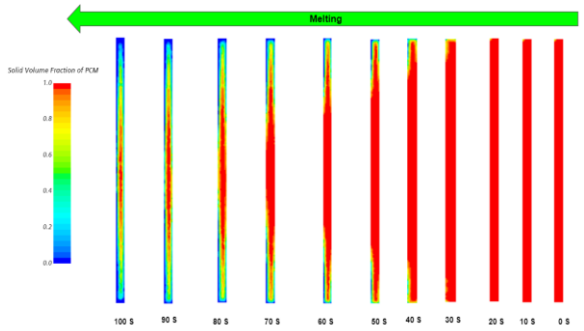

Figure 10. The volume fraction of 6 mm PCM configurations as a function of time

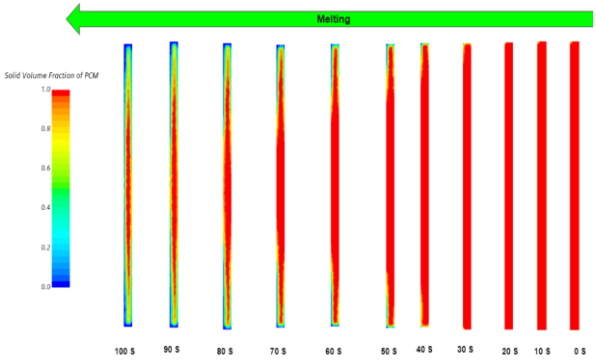

Figure 11. The volume fraction of 8 mm PCM configurations as a function of time

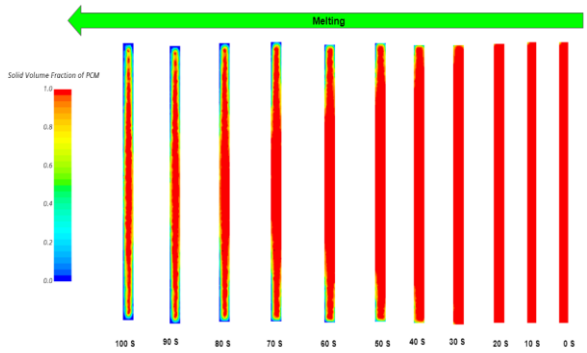

Figure 12. The volume fraction of 10 mm PCM configurations as a function of time

8. 2. Influence on Bracket Temperature for Different PCM Configurations The comparison of bracket temperatures for different PCM configurations was made to understand the thermal behavior. Three different PCM configurations were compared for temperature on the bracket, as shown in Figure 13. For

the first 10 seconds, the temperature of the bracket remains the same as the initial temperature. After 10 s, the temperature starts to increase. Every 5 seconds, the temperature of the bracket rises by 2 °C. For 20 seconds, the temperature of the brackets remains nearly constant across all configurations. After 20 seconds, the temperature of the bracket increases linearly, with 6 mm configurations having the lowest rate of temperature rise, followed by 8 mm configurations, and finally 10 mm configurations. From 0 s to 50 s, the temperature difference between the configurations is roughly 1 °C. After that, the temperature difference starts to increase from 2 to 5 °C. Based on the results, the best performing configuration is 6 mm, which is better in terms of volume fraction and temperature behavior. The initial temperature was 40 °C, and it ended with 78 °C, 82 °C, and 84 °C for three different configurations, i.e., 6 mm, 8 mm, and 10 mm configurations.

Different configurations' heat capacities were observed, as shown in Figure 14. The lowest heat transfer rate of 80 kW was observed for 6 mm configurations, and more than 100 kW was observed for 8 mm and 10 mm configurations, which means the amount of heat energy required to change the phase is reduced and heat is conducted through the brackets faster compared to other configurations. The volume fraction and temperature behavior results show that the 6 mm configuration performs better and helps to keep the temperature of the brackets as low as possible. Henceforth, the 6 mm configurations are simulated for cyclic load conditions.

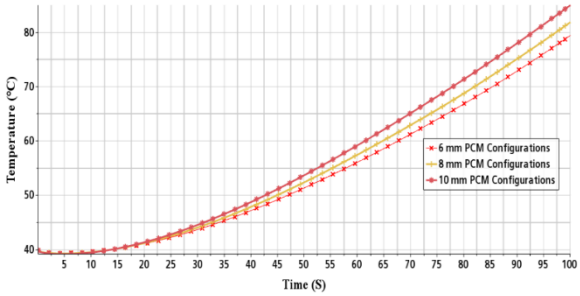

Figure 13. Bracket temperature of different PCM configurations as a function of time

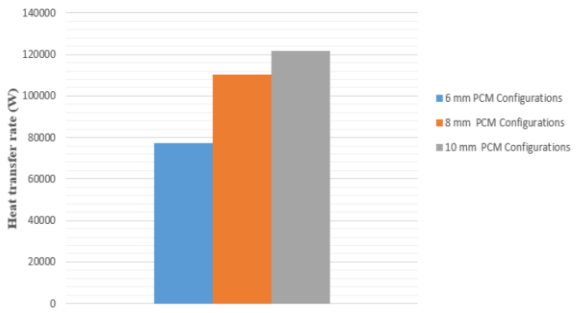

Figure 14. The heat capacity comparison of different PCM configurations

The primary liquid coolant was kept at an inlet temperature of 40 °C, and the outlet temperature was monitored for three different configurations as shown in Figure 15. According to the results, the temperature of 6 mm configurations is 79 °C, while that of 8 mm and 10 mm configurations is around 81 °C and 85 °C, respectively. The 10 mm configuration increases the overall temperature of the system when compared with the 8 mm and 6 mm configurations.

As shown in Figure 16, the PCM is unwrapped to demonstrate the thermal behaviours of various configurations. The lowest temperature is observed in 6 mm configurations, where we have the lowest temperature in the middle of the PCM and the highest temperature on the top and bottom of the wall. But when we study the other configurations, the bottom wall has a higher temperature, which shows the thermal gradient is higher and the uniform melting of PCM will not happen in the cases of 8 mm and 10 mm because of the difference in temperature between the top and bottom walls.

By comparing the bracket temperature results with previously published work [18,19] the present study shows better heat transfer, which results in lower bracket temperature as shown in Table 4.

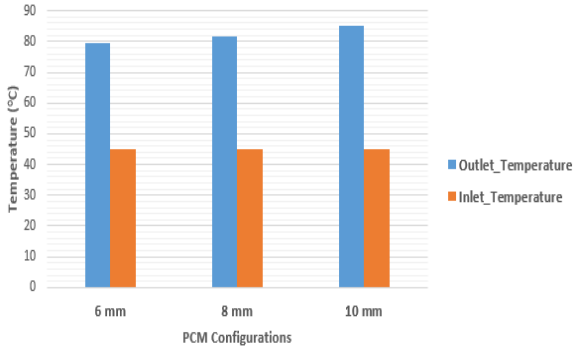

Figure 15. The Inlet and outlet temperature comparison for liquid coolant

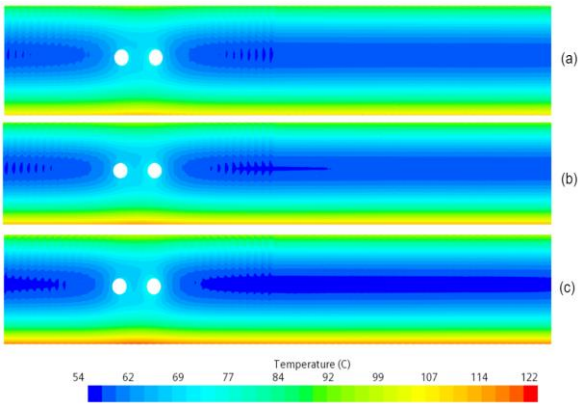

Figure 16. Different PCM configurations Unwrap (a) 6 mm (b) 8 mm (c) 10 mm are compared for temperature behavior

As explained in Figure 4, the heat transfer should happen from the stator to the ambient via brackets. In order to enhance the heat transfer, the PCM should convert the phase from solid to liquid faster so that the heat energy used for the phase change will be lower and the heat capacity will also be lower, enhancing the conduction within the solid and then to the ambient, which we can see in Figure 14 in terms of the heat capacity of the PCM. Based on the above results, the best-performing PCM configuration is 6 mm. The lower the thickness, the better the phase change of the PCM. An increase in the thickness of the PCM will not improve the heat transfer and is very ineffective, which means more heat energy will be stored within the system, which will increase the temperature of the brackets.

8. 3. Study of PCM Configurations with Cyclic Load Conditions Among the three different PCM configurations studied based on the results, the best-performing configuration is 6 mm. It is better in terms of heat transfer and latent heat. The simulations were performed for a period of 100 s to understand the best performing configurations. The aim of these studies is to understand PCM configurations that can effectively manage thermal loads. Now the cyclic load condition will be applied to study the heat transfer behavior and the volume change of PCM materials, as shown in Figure 17. The cyclic load conditions, PCMs are subjected to repetitive heating and cooling cycles. Understanding the behavior of PCMs under these conditions is crucial for optimizing their performance and ensuring efficient thermal management. The cyclic load conditions were performed for a period of 400 s, as shown in Figure 18, which is an ideal condition for motor operation to understand the behavior (20). The heat transfer varies between 1 and 9 kW.

Figures 18 and 19 show that under cyclic load conditions, the PCM almost remains solid until 100 s. For every additional 25 s, the phase change of an additional 10 % is noticed, which is a linear progression until 260 s. Almost 50 % of phase change happens at 200 s, and in another 120 s, complete phase change happens, which is faster when compared with the first phase of the melting process, which lasts until 200 s.

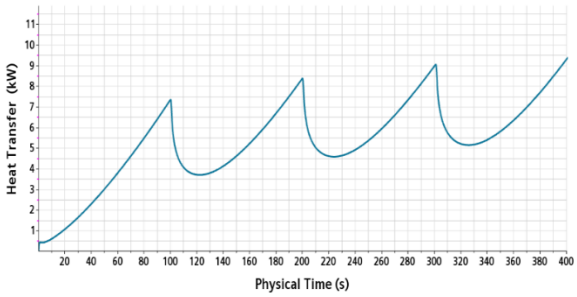

Figure 17. The 6 mm configuration applied with cyclic load conditions

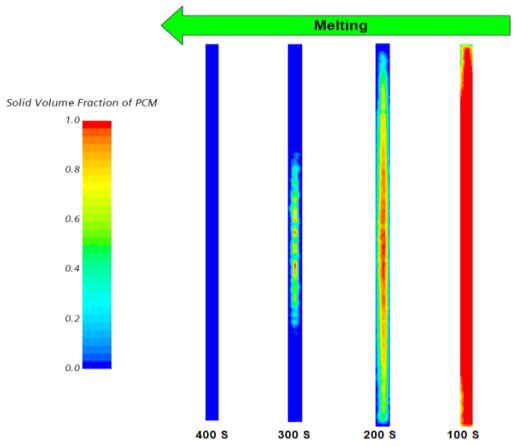

Figure 18. The volume fraction of 6 mm PCM configurations with a function of time

TABLE 4. Compassion with previous study

Bracket Temperature (°C) refereed from [18]	Bracket Temperature (°C) refereed from [19]	Bracket Temperature (°C) from present work
Liquid cooling method	PCM cooling method	Liquid & PCM cooling method
100 -120 (°C)	160 (°C)	80 (°C)

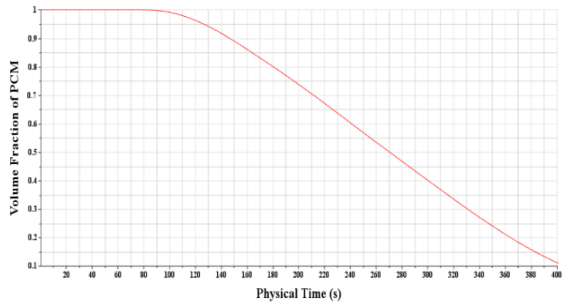

Figure 19. The volume fraction of 6 mm PCM configurations

The phase change of OM35 begins at 45 °C, where only a 1% change is observed. A bracket temperature of 76 °C causes a 50% phase change. The complete phase change happens at a temperature of 90 °C in 360 s. The temperature starts at 45 °C and rises to 100 °C after 400 seconds, as shown in Figure 20.

The PCM unwrap is to show the thermal behavior of the complete PCM from the inlet to outlet location. The bottom wall of the PCM is hotter when compared to the top wall. Under cyclic load conditions, unsymmetrical temperature distribution is observed, which results in the non-uniform melting of PCM, as shown in Figure 21.

The primary coolant unwrap shows a higher temperature at the center of the coolant passage. During cyclic load conditions, the highest temperature is observed in the center of the passage, where we have the outlet, and the coolant at a higher temperature. The non-uniform cooling observed in the PCM is due to heat transfer from the primary coolant, as shown in Figure 22.

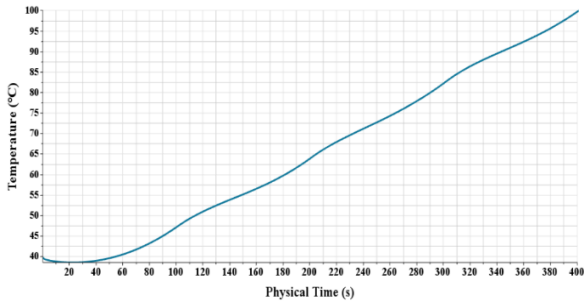

Figure 20. The thermal behaviour of 6 mm PCM configurations

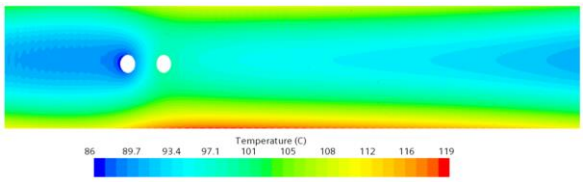

Figure 21. PCM unwrap for 6 mm configurations

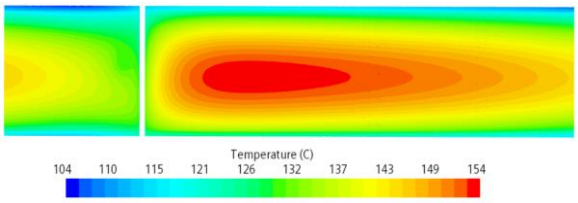

Figure 22. Primary Coolant unwrap for 6 mm configurations

9. CONCLUSION

The concept of the primary and secondary cooling systems of an e- machine works well and helps to keep the operating temperature within limits. The novel invention helps to reduce the bracket temperature from 120 °C to 80 °C, which is a significant improvement compared to other cooling techniques and is beneficial for the mild to hybrid categories of vehicle motor cooling.

In this study, the thickness of PCM, which acts as a secondary coolant, was studied, and it was found that the thickness of PCM will impact the temperature of brackets. Under constant load conditions, it took nearly 100 s to completely melt the PCM. The thicknesses of 6 mm, 8 mm, and 10 mm were studied, and it was found that the 6 mm thickness shows better results in terms of heat transfer and uniform cooling of brackets.

Under cyclic load conditions, the PCM of 6 mm configurations helps us maintain a uniform temperature of the brackets. Further studies could improve heat transfer by adding the baffles to the cooling channel.

10. REFERENCES

1. Lee K-H, Cha H-R, Kim Y-B. Development of an interior permanent magnet motor through rotor cooling for electric vehicles. Applied Thermal Engineering. 2016;95:348-56. 10.1016/j.applthermaleng.2015.11.022
2. Bellettre J, Sartre V, Biais F, Lallemand A. Transient state study of electric motor heating and phase change solid-liquid cooling. Applied Thermal Engineering. 1997;17(1):17-31. 10.1016/1359-4311(96)00026-9
3. Huai Y, Melnik RV, Thogersen PB. Computational analysis of temperature rise phenomena in electric induction motors. Applied Thermal Engineering. 2003;23(7):779-95. 10.1016/S1359-4311(03)00013-9
4. Boglietti A, Cavagnino A, Staton D, Shanel M, Mueller M, Mejuto C. Evolution and modern approaches for thermal analysis of electrical machines. IEEE Transactions on industrial electronics. 2009;56(3):871-82. 10.1109/TIE.2008.2011622
5. Hosain ML, Fdhila RB. Air-gap heat transfer in rotating electrical machines: a parametric study. Energy Procedia. 2017;142:4176-81. 10.1016/j.egypro.2017.12.343
6. Yabiku R, Fialho R, Teran L, Ramos ME, Kawasaki N. Use of thermal network on determining the temperature distribution inside electric motors in steady-state and dynamic conditions. IEEE Transactions on Industry Applications. 2010;46(5):1787-95. 10.1109/TIA.2010.2057398
7. Cavazzuti M, Gaspari G, Pasquale S, Stalio E. Thermal management of a Formula E electric motor: Analysis and optimization. Applied Thermal Engineering. 2019;157:113733. 10.1016/j.applthermaleng.2019.113733
8. Kuria J, Hwang P. Investigation of thermal performance of electric vehicle BLDC motor. International journal of mechanical engineering. 2012;1(1):1-17.
9. SC K, W K, MS K. Cooling performance of 25 kW in-wheel motor for electric vehicles. 2013. 10.1007/s12239-013-0060-9
10. Kim DG, Kim SC. An analysis study for thermal design of ISG (Integrated Starter & Generator) for hybrid electric vehicle. Transactions of the Korean Society of Automotive Engineers. 2013;21(4):120-7. 10.7467/KSAE.2013.21.5.145
11. SC K. Thermal Performance of Motor and Inverter in an Integrated Starter Generator System for a Hybrid Electric Vehicle. 2013. 10.3390/en6116102
12. Nategh S, Huang Z, Krings A, Wallmark O, Leksell M. Thermal modeling of directly cooled electric machines using lumped parameter and limited CFD analysis. IEEE Transactions on Energy Conversion. 2013;28(4):979-90. 10.1109/TEC.2013.2283089
13. Zhou K, Pries J, Hofmann H. Computationally efficient 3-D finite-element-based dynamic thermal models of electric machines. IEEE Transactions on Transportation Electrification. 2015;1(2):138-49. 10.1109/TTE.2015.2456429
14. DH L, SC K. Thermal performance of oil spray cooling system for in-wheel motor in electric vehicles. 2014. 10.1016/j.applthermaleng.2013.11.057
15. Huang J, Naini SS, Miller R, Rizzo D, Sebeck K, Shurin S, et al. A hybrid electric vehicle motor cooling system—design, model,

and control. IEEE Transactions on Vehicular Technology. 2019;68(5):4467-78. 10.1109/TVT.2019.2902135

16. Pechanek R, Bouzek L, editors. Analyzing of two types water cooling electric motors using computational fluid dynamics. 2012 15th International Power Electronics and Motion Control Conference (EPE/PEMC); 2012: IEEE. 10.1109/EPEPEMC.2012.6397424
17. Li H. Cooling of a permanent magnet electric motor with a centrifugal impeller. International journal of heat and mass transfer. 2010;53(4):797-810. 10.1016/j.ijheatmasstransfer.2009.09.022
18. Jayakumar S, Sreekanth M. A novel cooling method for electric vehicle motors–a CFD study.
19. Selvan J, Manavalla S. Numerical Analysis of E-Machine Cooling Using Phase Change Material. Energies. 2022;15(15):5594. 10.3390/en15155594
20. Durham MO, Lockerd CR. Effect of cyclic loading on motor efficiency. IEEE Transactions on industry applications. 1988;24(6):1153-9. 10.1109/28.17491
21. Pradeep R, Venugopal T. Experimental study of lithium-ion battery cooling using mixture of phase change materials. International Journal of Electric and Hybrid Vehicles. 2020;12(2):168-83. 10.1504/IJEHV.2020.10027333
22. Kumar S, Hassan SB, Sharma K, Baheta A. Heat Transfer Coefficients Investigation for TiO2 Based Nanofluids. International Journal of Engineering, Transactions A: Basics. 2019;32(10):1491-6. 10.5829/ije.2019.32.10a.19

Persian Abstract

چکیده

هوا، مایع و روغن معمولاً برای خنک کردن موتورهای وسایل نقلیه الکتریکی استفاده می شود. مواد تغییر فاز (PCM)جدا از قطعات الکترونیکی به طور گسترده مورد استفاده قرار نگرفتند. به طور کلی، خنک کننده هایی مانند هوا، مایع و روغن به طور جداگانه به عنوان خنک کننده مستقل برای موتور استفاده می شدند. در این تحقیق دو کانال خنک کننده به خنک کننده موتور اضافه شد. مایع به عنوان خنک کننده اولیه استفاده می شود، در حالی که PCM به عنوان خنک کننده ثانویه استفاده می شود. این روش جدید خنک‌سازی به حفظ دمای براکت در زیر حد مجاز کمک می‌کند، حتی اگر خنک‌کننده مایع در پایین‌ترین نقطه کار خود کار کند. در این مطالعه، تمرکز اولیه روی کانال خنک کننده PCM با نگه داشتن مایع خنک کننده مایع در یک شرایط عملیاتی خاص برای مطالعه جزئیات PCM بود. ضخامت PCM بر خنک کننده موتور تأثیر داشت. سه کانال PCM مختلف با ضخامت های ٦ میلی متر، ٨ میلی متر و ١٠ میلی متر مورد مطالعه قرار گرفتند. بهترین موارد با ضخامت PCM 6 میلی متر شناسایی شد که از نظر بهبود انتقال حرارت ٦ درصد مشاهده شد.